ESRF	**Experiment title:** Hierarchical structure of polymer/clay nanocomposites	**Experiment number**: SC-2316
Beamline: BM26B	**Date of experiment**: from: 24/11/2007 to: 26/11/2007	**Date of report**: 31-8-2008
Shifts: 6	**Local contact(s)**: Dr. Giuseppe Portale	*Received at ESRF:*

Names and affiliations of applicants (* indicates experimentalists):

Dr. LONGO Alessandro / ISMN-CNR, via Ugo La Malfa 153, I-90146, Palermo, Italy / +39-091-6809359 / alex@pa.ismn.cnr.it

Professor ANASTASIADIS Spiros / Dept. of Chemical Engineering, Aristotle University of Thessaloniki, 541 24, Thessaloniki, Greece / +30-2310-994245 / spiros@iesl.forth.gr

*PAVLOPOULOU Eleni / Foundation for Res. & Techn. - Hellas, P.O. Box 1527, GR-71110 Heraklion, Greece / +30-2810-391261 / epavl@iesl.forth.gr

*FOTIADOU Sapfo / Department of Chemical Engineering, Aristotle University of Thessaloniki, 541 24, Thessaloniki, Greece / +30-2310-996269 / sapfo@auth.gr

Report:

With this experiment we aim to estimate the structural properties of both the organic and inorganic components of polymer/clay nanocomposites and to investigate the effect of the presence of the inorganic component to the crystallization kinetics of the polymeric matrix. Three series of organic/inorganic nanocomposites were studied; a) polystyrene (PS) / Cloisite 20A intercalated nanohybrids containing 10 and 20wt% C20A, b) polypropylene grafted maleic anhydrite (PP-g-MAH) / Cloisite 20A exfoliated nanohybrids containing 5, 10, 20 and 40wt% C20A, and c) poly(ethylene oxide) (PEO) / Na^+ Montmorillonite (Na^+MMT) intercalated nanohybrids containing 1, 5 and 10wt% Na^+MMT. The pure PS, PP-g-MAH and PEO polymers were examined as well. The method that was used for the preparation of the series a) and c) was melt mixing. The two components were mixed and then annealed in a vacuum oven at a temperature higher than the polymer softening temperature for 2 days. The samples of series b) were prepared in a DSM micromixer- microextruder. X-ray Diffraction measurements were conducted to identify the intercalation/exfoliation.

SAXS data were recorded on a two-dimensional position sensitive detector using an X-ray wavelength of 1.55 Å. The sample-to-detector distance was set at 5 m and the scattering vector range explored was $0.06 < q < 1.2$ nm^{-1}. The two-dimensional images were radially averaged around the center of the primary beam, in order to obtain the isotropic SAXS intensity profiles. The scattering patterns from a specimen of wet collagen (rat tail tendon) and Silver Behenate were used for calibration of the q scale of the scattering profiles. The data have been normalized to the intensity of the incident beam (in order to correct for primary beam intensity decay) and corrected for absorption. Two ionization chambers placed before and after the sample, were utilized for the measurement of the incident and the transmitted beam. Two procedures for background correction were applied; i) subtraction of the air and empty cell contribution to scattering from the total intensity, and ii) subtraction of the “liquid-like” background, that is the scattering of the polymer melt. The latter is necessary for the correct calculation of the correlation function and ensures the

dissociation of the contribution of the clay to the scattering pattern and the isolation of the polymer scattering. The samples were placed inside aluminum pans and a Linkam hot stage was used for the temperature control. Time resolved measurements were performed on the PEO nanocomposites in order to record the lamellar formation and growth in the presence of the inorganic components. The samples were annealed at 100°C, above the melting temperature, T_m, kept there for 5 min and, after the acquisition of the melt scattering pattern, they were quenched at 30°C/min at different isothermal crystallization temperatures, T_{IC}, a few degrees above the non-isothermal crystallization temperature T_C. For the nanocomposites, T_{IC} varied between 46°C and 52°C by a step of 1°C, while for the net PEO this range was extended down to 42°C due to its lower T_C. Sequential SAXS patterns were acquired, following the isothermal crystallization at the respective T_{IC}. Data collection was started on reaching the isothermal temperature over consecutive acquisition time lapses of 15s, and was stoped a few minutes after the stabilization of the traces of the total scattered intensity and the transmission that were simultaneously monitored during the measurement, which is considered to be indicative of the end of the crystallization procedure. We note that certain extra measurements needed in order to complete this project were conducted or repeated during our scheduled beamtime SC-2481 on April 2008, in the same beamline, under the same experimental conditions.

The scattering patterns acquired for the pure PS and the 10wt% Cloisite 20A containing nanocomposite are presented in Fig.1. The two curves are very similar and no characteristic feature related to the clay contribution to the scattering is observed (the 2D SAXS data did not show any indication of platelet alignment because of the sample preparation method). Thus, no estimation on the characteristics of the ordered stacks of clay platelets is considered to be possible. Probably the contribution of the clay to the total scattering is restricted to a constant background at the q range under study, due to the large dimensions of the platelets with respect to the lengthscales probed by SAXS. This conclusion is further reinforced by the scattering patterns of the pure PEO and the corresponding nanocomposites, which are identical.

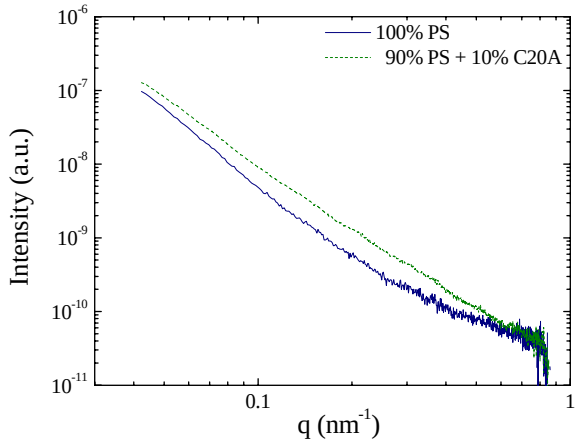

Figure 1: The SAXS intensity curves for the pure PS and the 90% PS – 10 % Cloisite 20A nanocomposite.

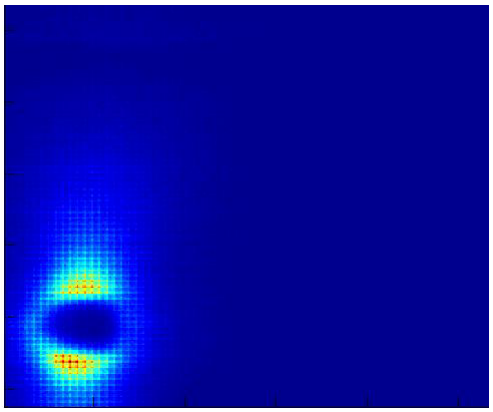

Figure 2: The 2D SAXS image acquired for the 90% PP-g-MAH – 10% Na^+MMT nanocomposite.

Figure 2 presents the 2D SAXS image that corresponds to the 90% PP-g-MAH – 10% C20A nanocomposite. The apparent anisotropic scattering was not eliminated after annealing above the melting temperature of PP-g-MAH, which implies that it is due to alignment of the inorganic component. Similar results were obtained for all the compositions under study. This anisotropic scattering was attributed to the sample preparation method applied, since the clay platelets tend to orient during the extrusion parallel to the extrusion direction, and thus the background scattering from the clays changes with the orientation of the scattering vector. We did not proceed with the time resolved measurements for the investigation of the crystallization of the PP-g-MAH nanocomposites since we first wanted to understand how to dissociate the polymer contribution to the total scattering from such an anisotropic pattern.

Figures 3 shows the scattering patterns collected during the isothermal crystallization at 47°C of the nanocomposite with 90% PEO – 10% Na^+MMT (a) and the corresponding Lorentz corrected curves (b). The initial scattering patterns acquired during the isothermal crystallization correspond to those of the melt state of the amorphous polymer in the nanohybrid. After a while, a broad peak appears at 0.28nm^{-1} approximately, corresponding to a lamellar period of 22nm. The intensity of the peak increases during crystallization and

then remains constant. The patterns of all the nanocomposites at various T_{IC} were similar, however differences were observed in the peak position, the intensity and the evolution time of the crystallinity peak. For example, the dependence of the crystalline long period (d^*) on the clay content and the crystallization temperature is presented in Fig. 4. Herein, the long period is derived by the peak position of the Lorentz corrected curves, however the correlation function analysis that is curently applied on our data is expected to provide us with more accurate results concerning the thicknesses of the crystalline lamellae and the amorphous regions as well as with the crystallinity of our samples.

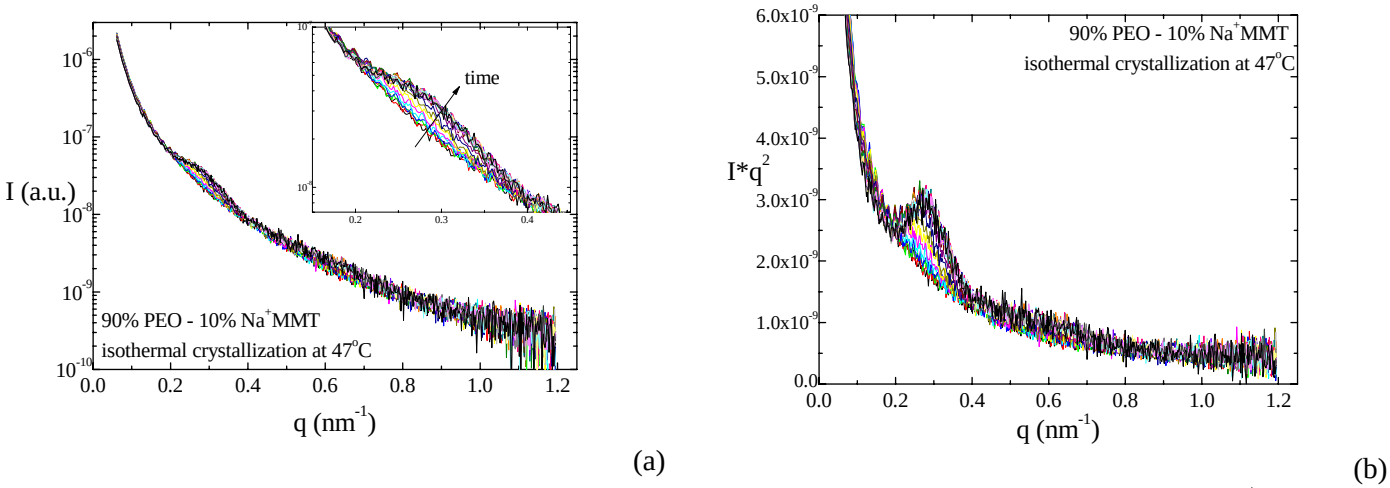

Figure 3: Time resolved SAXS patterns acquired during the isothermal crystallization of the 90% PEO - 10% Na^+MMT nanocomposite at 47^{o}C (a) and the corresponding Lorentz corrected patterns (b).

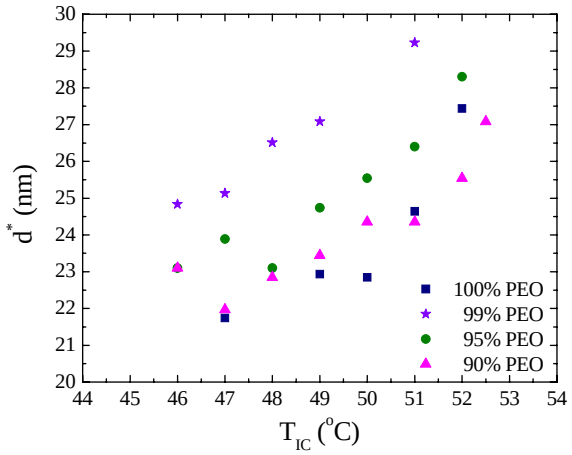

Figure 4: The long period, d^*, of the crystals formed for the various compositions as a function of the isothermal crystallization temperature T_{IC}.

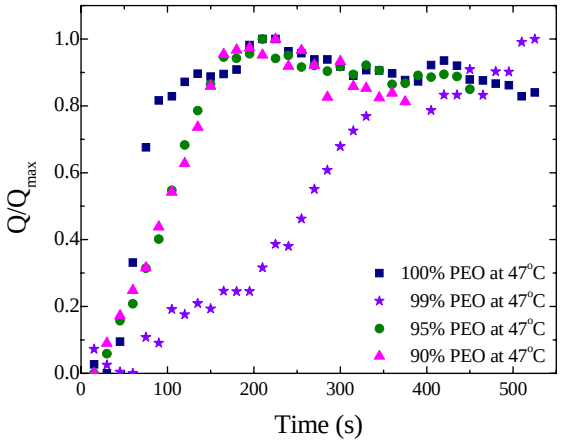

Figure 5: The evolution of the invariant during the time resoved measurements for the pure PEO and two nanocomposites, for T_{IC} = 47^{o}C. The values

Moreover, the time resolved measurements can inform us about the time $t_{1/2}$, that is related to the time required for the 50% completion of the crystallization procedure, and the nucleation mechanism, by appropriate utilization of the Avrami equation. This is manifested in Fig. 5, where the invariant, Q, (normalized by its initial value in order to facilitate the direct comparison between the samples) is plotted versus time of the time-resolved measurements. We can see that, at this particular temperature, the crystallization kinetics slows down with the incorporation of the inorganic component. The change in the slope during the initial stages of the crystallization is related to the possible change of the nucleation mechanisms.

Although the analysis of the data acquired during this experiment is still ongoing, the results obtained so far concerning the crystallization of the PEO nanocomposites are very promissing and at least one publication is foreseen.